atmosphere

MDPI

Article

The Seasonality of PM and NO_2 Concentrations in Slovakia and a Comparison with Chemical-Transport Model

Tereza Šedivá [1,2] and Dušan Štefánik [2,*]

[1] Faculty of Mathematics, Physics and Informatics, Comenius University in Bratislava, Mlynská Dolina F1, 842 48 Bratislava, Slovakia; tereza.sediva@fmph.uniba.sk
[2] Slovak Hydrometeorological Institute, Jeséniova 17, 833 15 Bratislava, Slovakia
* Correspondence: dusan.stefanik@shmu.sk

Abstract: The air quality (AQ) of a given location depends mostly on two factors: emissions and meteorological conditions. For most places on Earth, the meteorology of an area changes seasonally. For central Europe, winters are associated with poor dispersion conditions, which, in combination with high emissions from local heating systems, lead to significantly higher concentrations than during summer. In this study, the seasonality of AQ is analysed using hourly measurements from 44 monitoring stations in Slovakia for the years 2007–2023 for NO_2, PM_{10} and $PM_{2.5}$. Two factors are used to evaluate the seasonality—the difference and ratio of the winter and summer mean concentrations. It was found that the seasonal difference has been gradually decreasing for all pollutants since 2017. In the case of $PM_{2.5}$, the seasonal ratio drops from a value of around 2.5 in 2018 to approximately 1.7 in 2023. While in the past, the seasonal ratio was the highest for $PM_{2.5}$, in the last three years it is the highest for NO_2 with values larger than 2. Our results imply that summer sources of PM emissions start to play a more important role for the AQ than in the past. The observed seasonality was compared with two full-year chemical-transport model simulations.

Keywords: air quality; air quality modelling; seasonality of air quality; chemical-transport modelling; pollutant concentrations; meteorology

check for updates

Citation: Šedivá, T.; Štefánik, D. The Seasonality of PM and NO_2 Concentrations in Slovakia and a Comparison with Chemical-Transport Model. *Atmosphere* **2024**, *15*, 1203. https://doi.org/10.3390/atmos15101203

Academic Editors: Adrianos Retalis, Vasiliki Assimakopoulos and Kyriaki-Maria Fameli

Received: 30 August 2024
Revised: 3 October 2024
Accepted: 6 October 2024
Published: 8 October 2024

Copyright: © 2024 by the authors. Licensee MDPI, Basel, Switzerland. This article is an open access article distributed under the terms and conditions of the Creative Commons Attribution (CC BY) license (https://creativecommons.org/licenses/by/4.0/).

1. Introduction

The air quality (AQ) has been recognized as a threat to human health for centuries [1] and still remains the biggest environmental risk to health globally [2]. Many studies have shown the direct effects of pollutants such as particulate matter (PM) [3,4], ozone (O_3) [5] or nitrogen oxides (NO_x) [6,7] on human health. Despite gradual improvements in the AQ in Europe, the concentrations of pollutants commonly exceed AQ standards and are often well above the WHO guidelines [8]. Therefore, the AQ remains a relevant topic to this day.

The AQ of an area is usually assessed by measuring pollutant concentrations in the air. The level of concentrations of any pollutant depends on many factors, mainly the emissions, chemical creation, and depletion of the pollutants in the atmosphere, as well as various physical processes which affect the transport of pollutants. These are mainly the dispersion and diffusion of pollutants by the wind field, but also wet and dry depositions. These influences are generally changing in time, which affects the concentration levels at any given time and space. The wind flow is to a great extent affected by the orography of a given area. The configuration of urban settlements also has a significant effect on the AQ, mainly within densely populated cities [9,10]. The emissions of most pollutants have specific time profiles on diurnal, weekly and annual scales, which mostly depend on societal behaviour (e.g., commuting in the morning and evening during weekdays but not on weekends) and seasonal changes (e.g., temperature changes and sunlight). The seasonal weather changes also directly affect the dispersion conditions. The seasonal AQ changes based on the combined effects of weather and emissions are what we refer to as the seasonality of AQ.

The seasonal changes in the AQ have been studied in many countries, in many different local climates. The studies focus mainly on seasonal changes of concentrations in the selected region, and the correlation of the concentrations of various pollutants with meteorological parameters (mainly temperature, wind speed and wind direction) and other pollutants [11–14]. Some studies have used large amounts of stations [13] or low-cost sensors [15] to evaluate the seasonal patterns. Another has also focused on diurnal profiles of the AQ [16] and their seasonal variation [17]. The studies clearly show that the meteorological conditions play an important role in determining the resulting AQ [18], and that the seasonality of AQ is strongly dependent on the specific local circulation [19]. The results of country-specific studies hence cannot be applied globally.

In this paper, the seasonality of AQ is analysed at 38 National Air Quality Monitoring Network (NMSKO) sites, which are operated by the Slovak hydrometeorological institute (SHMU), and six private stations. Not all stations were used for all pollutants. The seasonality is presented for PM_{10} and NO_2 for the years 2007–2023 and for $PM_{2.5}$ for the years 2017–2023. Apart from the analysis of the observed seasonality, the paper also covers seasonality computed with chemical-transport model CMAQ for the years 2017 and 2023 for the region of Slovakia. Model CMAQ is a regional, Eulerian, open-source model [20], which is widely used within the AQ modelling community. At SHMU, the model CMAQ is used for the operational forecast of pollutant concentrations in Central Europe [21], and to a lesser extent for source apportionment and other research. Since the model is routinely used at SHMU, the evaluation of the model's capacity to capture the seasonal differences in Slovakia is important for future assessment of predictions.

The air quality monitoring stations provide the most reliable information about concentrations of pollutants in the atmosphere. The disadvantage of point measurements at station locations is that they are influenced by local sources and effects, and hence they may not reflect the actual pollution levels that people are exposed to in everyday life. Hence, the seasonality calculated from the measurements is often site-specific. Air quality models and satellite measurements provide spatial distribution of concentrations for large areas, which allows us to calculate the seasonality for areas not covered by the stations, but limited by the resolution of the model or satellite. The main disadvantage of satellite data is that they provide concentrations for the whole depth of the atmosphere or troposphere, which might not reliably reflect the observed concentrations near the ground. Further, a lot of satellite data are missing due to the presence of clouds. In Slovakia, more cloud cover occurs during winter in comparison to summer, which presents another challenge for studying the seasonality by satellites due to uneven availability of data during analysed periods. On the other hand, the air quality models provide concentrations of pollutants for every grid cell of the model domain at every time step, but the accuracy of the results is strongly dependent on the meteorological and emission inputs. For the accurate calculation of seasonality in the models, emission time profiles must properly reflect the real emission variation.

The main goals of this work are to evaluate the trends in the observed seasonality in Slovakia and the ability of the AQ model CMAQ (the current and previous setup) to capture the observed seasonality. The model results will further provide approximate information about the seasonality of AQ in areas not covered by the measurements. There have not been any such studies observing the trends in seasonal changes of the AQ in Slovakia, nor a comparison of the models. Additionally, analysis of the model results allows future improvements of the model, by providing a first step in detecting the seasonal differences in model performance.

Air Quality and Its Seasonal Variation in Slovakia

Slovakia is located in Central Europe with four distinct seasons throughout the year—spring (March to May), summer (June to August), autumn (September to November) and winter (December to February). It is characterized by diverse orography with large lowlands in the south of the eastern and western parts of the country and mountainous areas in the northern and central parts (Figure 1). The AQ of Slovakia has been slowly improving as

the emissions of basically all pollutants have been steadily decreasing from 1990 [22]. It is assumed that climate change also contributes to the decrease in emissions due to higher temperatures during the cold months of the year and hence a shorter heating season and a lower need for heating in general [23]. This poses the question of whether the patterns of the AQ throughout the year are slowly changing as well.

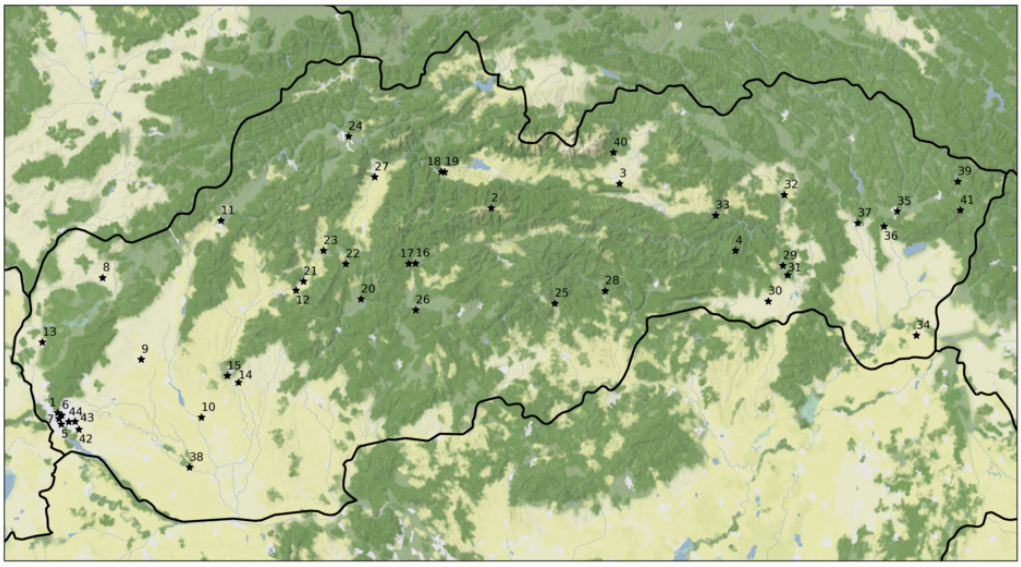

Figure 1. Terrain of Slovakia. The dots indicate the positions of AQ monitoring stations used in the analysis. The list of stations labelled by numbers can be found in Table A1 in Appendix A.

The main pollutants of concern in Slovakia are PM_{10} (PM with diameter smaller than 10 µm, $PM_{2.5}$ (PM with diameter smaller than 2.5 µm) and NO_2 (nitrogen dioxide). The main source of PM is residential heating, which provides thermal energy for heating and cooking. In 2021, residential heating produced more than 81% of the total annual $PM_{2.5}$ [22]. In 2018, residential heating comprised around 75% of $PM_{2.5}$ emissions and almost 60% of the PM_{10} emissions in Slovakia [24]. Based on data from [22], 38% of the energy consumption in Slovakia in 2021 for residential heating category can be attributed to solid fuels, with firewood being the most used with an energy consumption of 86% of the solid fuels. Residential heating emissions are directly determined by the temperature of the air, as it changes throughout the year. The official heating season lasts from September to May, and typically starts with average daily temperature below 13 °C [25]. However, due to climate change, the number of heating days has been decreasing and is predicted to further decrease, mainly in May and September [25].

NO_2 is mainly created in the atmosphere from the emissions of NO_x, which originate primarily in the traffic and industrial sectors. NO_x is a family of seven compounds, but only NO_2 is EPA-regulated, because it is the most prevalent of the compounds of anthropogenic origin [26]. The emissions of NO_x from combustion are primarily in the form of NO [26], and the NO_2 is then mostly created in the atmosphere by oxidation of NO [27]. In 2018, the main sources of NO_x emissions in Slovakia were the traffic sector (around 40%) and industrial burning (14%) [24]. Other industries and agriculture both produced around 11%, while residential heating only contributed around 5% [24]. In 2021, the NO_x emissions reached 17.4 kt from road transport and 3.8 kt from heating [22]. For comparison, emissions of both PM_{10} and $PM_{2.5}$ from residential heating were around 15 kt.

The seasonality of AQ in Slovakia is apparent when comparing the winter vs. summer concentrations of pollutants. In winter, a combination of a more stable atmosphere and higher emissions of pollutants from residential heating during the heating season leads to higher levels of concentrations of PM_{10}, $PM_{2.5}$, NO_2 and other pollutants. Poor AQ often occurs especially in settlements situated in deep valleys in which the burning of solid

fuels is the main source of heat. Valleys are typically more prone to temperature inversions during the winter, which increases the stability of the atmosphere and causes bad dispersion conditions. During the summer, the dispersion in the atmosphere is generally favourable due to excessive turbulence, and there are almost negligible emissions from heating, leading to lower levels of concentrations. As will be further presented in Section 3.1, the differences between the average winter and summer concentrations have been steadily decreasing, and hence the seasonality of AQ on national level becomes less distinct. However, short episodes with very high PM concentrations still occur, almost solely in the colder period of the year.

2. Materials and Methods

To statistically evaluate the seasonality of AQ in Slovakia, winter and summer seasons are compared, due to their very different meteorological conditions and emission sources. In winter, local heating is the most important emission source of PM, while in summer, this source is almost negligible. Residential heating also contributes considerably to emissions of NO_x in winter, while the other sources of NO_x are mostly the same throughout the year. Combined with frequent poor dispersion conditions in winter in contrast with unstable conditions during summer, which lead to better ventilation, the choice of these two seasons is natural for the analysis of the seasonal patterns in AQ for Slovakia. This comparison can further provide insights into the effects of local heating systems on PM concentrations. Two simple factors were defined to evaluate the differences between these two seasons. The first one is a ratio of mean winter concentrations $\bar{c}_w$ of a pollutant to mean summer concentrations of the same pollutant $\bar{c}_s$

$$f_{ws} = \bar{c}_w / \bar{c}_s. \quad (1)$$

The second factor is a difference between the mean winter and summer concentrations

$$d_{ws} = \bar{c}_w - \bar{c}_s. \quad (2)$$

The f_{ws} tells us how much larger the winter concentrations are compared to the summer ones, while d_{ws} tells us the actual difference between the winter and summer concentrations in $\mu g \cdot m^{-3}$. To compute $\bar{c}_w$, the January, February and December of a given year are taken. To compute $\bar{c}_s$, June, July and August are taken.

2.1. Observed Seasonality

The seasonality of AQ is analysed at 38 NMSKO stations operated by the SHMU and 6 sites operated by private industrial companies. Table A1 in Appendix A includes the list of all stations used for the analysis. Figure 1 shows the position of each station in Slovakia. For the whole analysis, only stations with at least 75% of data for any given analysed period were used and included in the graphs. Only stations with 75% coverage for both summer and winter seasons concurrently were used for the computation of the seasonal factors.

For the purpose of the comparison of model results with observations, the station types (background, traffic, industrial) and locations (urban, suburban, rural) are used since some types are generally more comparable to the model results than others. The model only provides one average concentration for the whole grid cell and cannot capture gradients in concentrations on the sub-grid level. The traffic and industrial sources, which are positioned near larger emission sources, measure the peak in concentrations that the model cannot resolve. The background stations are characterized by not having a large emission source in their vicinity, and hence, they represent the average AQ over a larger area and are the most suitable to compare with a regional model. For our analysis, we divided the stations into the following groups:

(1) RB—rural background stations,
(2) SB—suburban background stations,
(3) UB—urban background stations,

(4) T—traffic stations,
(5) I—industrial stations.

We did not divide the T and I stations further based on their location, since near the vicinity of the source, the general character of the wider surroundings is less important.

2.2. Modeled Seasonality

The concept of the seasonality of AQ can also be studied with AQ models. Particularly in our case, we want to evaluate the capacity of an AQ model to effectively capture the seasonality of AQ similarly to the observations. Since the seasonality depends on both meteorology and emissions, the modelled seasonality depends on both the meteorological inputs and the temporal distribution of emissions. The model mechanism also affects the results, but here, we focus on how different inputs to the same model will affect its performance, rather than choosing a different model. The meteorological inputs are usually taken from the weather forecast and are assimilated by the real observations. Although the models predict the standard meteorological parameters like temperature, pressure and humidity quite well, the accuracy of the meteorological model might not be sufficient for the realistic computation of AQ. This is mainly due to the horizontal resolution, since there are often steep concentration gradients around emission sources or complex terrain which affects the AQ. The resolution in the vertical resolution is also often not fine enough to reliably capture the temperature inversions near the ground, the correct height of the boundary layer of atmosphere, or the stability class of the boundary layer. This might strongly affect the dispersion conditions in the model and hence lead to unrealistic results of the concentration fields.

With emissions, the task is even more complicated, since the emission data are seldom as detailed and accurate as the meteorological data. Apart from large industries that are required to report the emitted amounts of pollutants, the emissions of most emission sectors are usually not measured but are computed based on activity data and other proxy data. These computations typically require a lot of estimations, for example, of the consumption of specific fuel types or energy demand. Moreover, the emission estimates often cover larger time periods and do not give information about the specific pollutants that are being emitted, nor the temporal profiles of these emissions. The emission input fields are typically the main cause of uncertainty for the model simulations, and hence they will directly affect the model seasonality of the AQ.

In our analysis, we compare the observed seasonality with model CMAQ simulations for the years 2017 and 2023. Both simulations were previously computed at SHMU for different purposes with a time difference of computation of 5 years. Hence, both simulations use a different domain, meteorological, and emission inputs, depending on the practices used at the time of the computation. This comparison allows us to evaluate the improvement in the capability of the current model setup to capture the seasonality of AQ compared to the previous setup. The modelled seasonal factors f_{ws} and d_{ws} were computed for the grid cells in which the monitoring stations were located.

2.3. Simulations Specification

The 2017 simulation was computed with CMAQ version 4.7.1 [28] using a computational domain called "d02" (Figure 2a), with a 4.7 km horizontal resolution. The CB05 gas-phase chemistry mechanism [29] and the AERO4 version of the aerosol module [30] were used. The meteorology for the model was simulated with the WRF model version 3.9.1 [31]. The model WRF is widely used in union with the model CMAQ and other chemical transport models for a wide range of applications [32–34]. It has also been used in recent interesting studies, which improve the model results by the application of machine learning [35] and satellite data [36]. Reanalysed meteorological data from the European Centre for Medium-Range Weather Forecast (ECMWF) were used as the boundary and initial conditions. The emissions from residential heating were computed bottom-up for municipalities in Slovakia for 2017 [37]. The annual variation in this emission profile is the same for

all grid cells, and it is computed using the mean temperature of the whole domain according to the methodology implemented in FUME emission processor [38,39]. Other emissions (traffic, agriculture, industry) in the domain are from the TNO MAC-III 2015 database [40] and have their specific temporal profiles (annual, weekly and diurnal) adapted from [41]. The chemical boundary conditions (BC) are taken from a CMAQ simulation of a larger domain with a spatial resolution of 14.1 km, which covers a substantial part of Europe. The CMAQ default chemical BC for clean air were used for the outer domain.

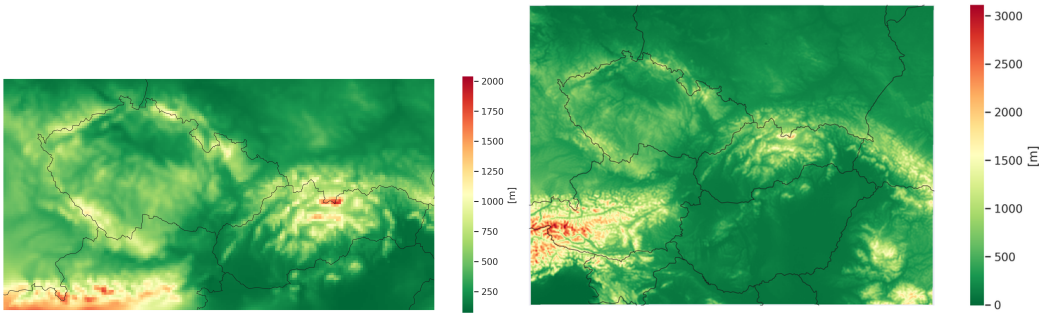

(**a**) d02 (**b**) ala2km

Figure 2. Two model domains, used for the 2017 and 2023 simulations, respectively.

The 2023 simulation was computed with CMAQ version 5.3.3 [20] using a computational domain called "ala2km" (Figure 2b), with a 2 km horizontal resolution. Carbon Bond 6 version r3 [42] and AERO7 [43] mechanisms were used for the gas-phase and aerosol chemistry, respectively. The meteorology for this model simulation was provided by the model ALADIN, which is the operational meteorological model run at SHMU [44]. The chemical BC were taken from the CAMS GLOBAL [45] and CAMS EUROPE models [46] . The traffic emissions in Slovakia were calculated based on the traffic intensity data for 2019, provided by the Transport Research Center (Centrum dopravního výzkumu, v. v. i.) [47]. Residential heating emissions for Slovakia were calculated with a bottom-up methodology [37] for 2021. These emissions were reggrided using the ZBGIS buildings layer [48]. Data for around 400 most important industrial point sources were taken from the Slovak National Emission Information System database [49]. The emissions from agriculture in Slovakia were based on 2018 national data and reggrided according to various proxy data, i.e., ZBGIS agriculture buildings and Corine landcover [50]. The emissions outside Slovakia were taken from the CAMS emission database CAMS-REG-ANT ver. 6.1-Ref_2022 [51]. The biogenic emissions for the whole domain were taken from model MEGAN (Model of Emissions of Gases and Aerosols from Nature) [52] using 2023 meteorological data from the model ALADIN.

2.4. Validation of Model Results

The results for both model simulations are presented in Table 1. The results were computed from hourly data from background stations only and are presented for summer and winter seasons and the whole year. The following evaluation statistics are used: correlation coefficient (R), mean bias (MB) and root mean square error (RMSE). The observed mean concentration values are presented (obs. mean) as well as the number of available stations for each pollutant and year (n). The MB, RMSE and obs. mean values are in $\mu g \cdot m^{-3}$.

Firstly, we can see a large difference between the observed winter concentrations in 2017 and 2023. In 2017, an unusually cold January resulted in higher heating demand and larger concentration values of pollutants. This January, which was the coldest in 30 years, was caused by a combination of factors: an intrusion of cold arctic continental air mass over Slovakia, the presence of snow cover over the land, a stable high-pressure region over Central Europe, and the frequent occurrence of low-level temperature inversions [53]. Approximately −5 °C deviation from the 1991–2020 period was recorded at most clima-

tological stations in Slovakia for the monthly mean temperature. This resulted in a large bias of model CMAQ for this month, which affected the statistics for the winter of 2017. The model was not capable to predict the high concentrations caused by a combination of frequent inversions and very stable weather, most probably due to insufficient resolution of vertical layers in the planetary boundary layer, which resulted in higher dispersion and lower concentrations within the model.

Table 1. Validation of 2017 and 2023 simulations for background stations.

Year	Pollutant	Period	n	Coverage [%]	Obs. Mean	R	MB	RMSE
2017	PM_{10}	summer		97.4	16.5	0.22	− 13.16	16.01
		winter		95.3	41.44	0.46	−31.14	44.27
		year	21	97.5	24.36	0.52	−17.81	26.67
	$PM_{2.5}$	summer		95.7	9.54	0.19	−6.37	8.99
		winter		95.5	35.75	0.45	−25.72	37.48
		year	21	95.7	18.27	0.54	−11.94	21.04
	NO_2	summer		91.5	7.21	0.44	−4.81	8.9
		winter		94.3	20.3	0.48	−13.61	21.23
		year	15	93	12.43	0.54	−8.02	14.14
2023	PM_{10}	summer		98.6	15.53	0.56	−8.09	10.86
		winter		98.9	21.33	0.57	−7.34	16.02
		year	34	97.7	16.85	0.59	−7.17	12.48
	$PM_{2.5}$	summer		98.2	10.78	0.54	−4.72	7.42
		winter		98.9	18.95	0.56	−5.17	14.69
		year	31	97.9	12.95	0.60	−4.21	10.01
	NO_2	summer		95.2	5.98	0.34	−2.54	5.42
		winter		95.7	14.20	0.50	−5.12	11.54
		year	25	93.6	9.34	0.56	−3.71	8.49

Looking back at the results, we see that the 2023 simulation agrees with the observations much better than the 2017 simulation for all three pollutants, mainly for PMs. For PMs, the correlation of the model has improved the most for the summer: 0.22 and 0.19 in 2017 compared to 0.56 and 0.54 in 2023, for PM_{10} and $PM_{2.5}$, respectively. The correlation for winter and for the whole year improved less, but still substantially. The correlation of NO_2 was actually better in the summer for 2017 (0.44, compared to 0.34 for 2023), while the results for winter and the whole year are only slightly better for 2023.

In terms of the model bias, the MB of the 2017 simulation was substantially reduced with the 2023 simulation, most evidently for the winter. The MB of the model is the largest for PM_{10}, but PM_{10} also reached the highest concentrations for these pollutants. Since each pollutant has a different observed mean and even for the same pollutant the observed concentrations are very different for these 2 years, it is best to look at the bias relative to the corresponding observed mean. For PM_{10}, the MB reaches, on average, 76% of the observed mean for 2017 and only 43% for 2023. For $PM_{2.5}$, it is 68% of the observed mean for 2017 and 35% for 2023, and for NO_2, it is 66% of the observed mean for 2017 and 39% for 2023. The RMSE is, as a percentage, the largest for NO_2 (114% of the observed mean for 2017 and 88% for 2023), compared to PM_{10} (104% of the observed mean for 2017 and 73% for 2023) and $PM_{2.5}$ (105% of the observed mean for 2017 and 75% for 2023).

Overall, the 2023 model setup performs significantly better. The largest improvement in the setup probably comes from its finer resolution (4.7 vs. 2 km); however, all aspects of the newer model setup improved, including the meteorology, emissions and boundary conditions. All of these improvements undoubtedly led to better performance of the current setup.

3. Results

3.1. Observed Trends in Seasonality and Seasonal Factors

The seasonal and annual mean concentrations for NO_2, PM_{10} and $PM_{2.5}$ are presented in Figures 3–5, respectively, for the whole analysed period. The values in the figures were

obtained as the mean from the measured values from the stations described in Section 2.1. Only years with at least 10 sufficient stations were included in the graphs. The data are presented since 2007 due to the higher number of available stations compared to previous years. For $PM_{2.5}$, a lot of data are missing before 2017, since most stations started to measure $PM_{2.5}$ just from this year. One can see that for all of these pollutants, the mean annual concentrations, as well as seasonal means, mostly gradually decreased during the given time period. The high peak in winter concentrations of PMs in 2017 (and to a lesser extent for NO_2) was caused by higher heating demand and the occurrence of strong low temperature inversions during the exceptionally cold January of 2017.

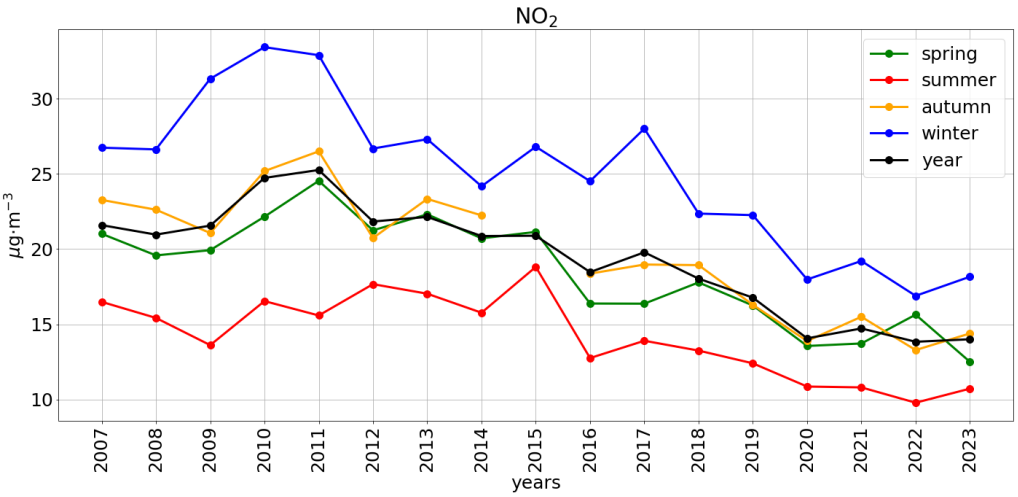

Figure 3. Average seasonal and annual concentrations of NO_2 at monitoring stations.

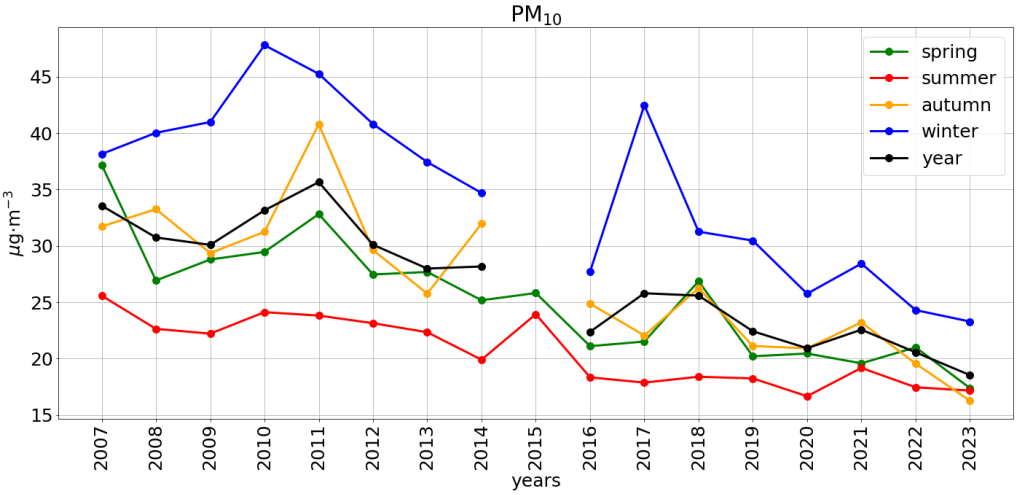

Figure 4. Average seasonal and annual concentrations of PM_{10} at monitoring stations. Missing data are due to fewer than 10 stations with the required coverage being available.

The ratio of winter to summer mean concentrations of f_{ws} is presented in Figure 6. For the NO_2, we can see that the f_{ws} does not show a clear trend, but it becomes quite stable around value 2.1 since 2018. On the other hand, for both PMs, we can see a gradual decrease in f_{ws} since 2017. This results from the fact that while for NO_2 both summer and winter concentrations have been steadily decreasing from 2017, for PMs only the winter concentrations have been decreasing, while the summer concentrations are nearly constant (see Figures 3–5).

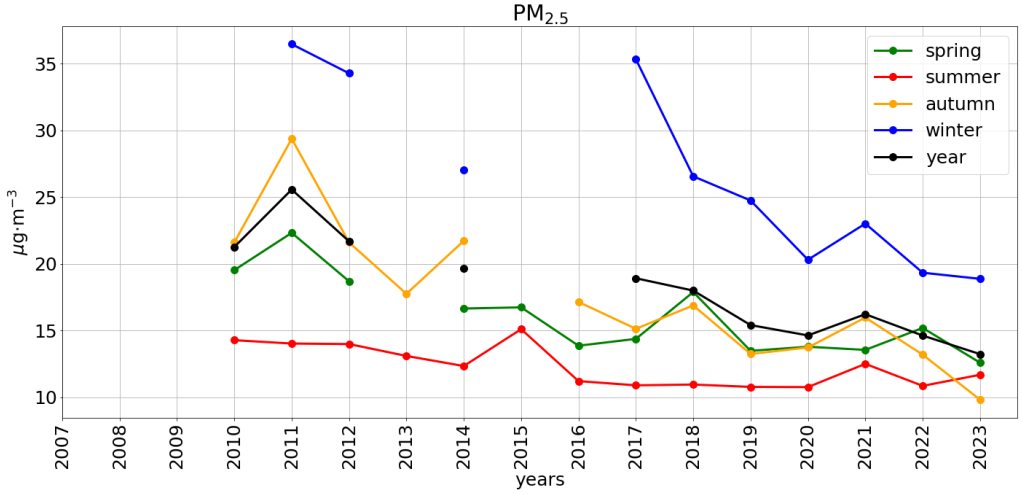

Figure 5. Average seasonal and annual concentrations of $PM_{2.5}$ at monitoring stations. Missing data are due to fewer than 10 stations with the required coverage being available.

The difference between winter and summer mean concentrations d_{ws} shown in Figure 7 has been mostly declining since 2010 and especially since 2017. In the case of NO_2, the d_{ws} has been almost constant for the last four years. The highest d_{ws} can be seen for $PM_{2.5}$, followed by slightly smaller values for PM_{10}. In Figure 6, we can also see that the f_{ws} for $PM_{2.5}$ is much larger than for PM_{10}. These results show that it is the fine fraction of PMs—$PM_{2.5}$—which causes the differences between the winter and summer concentrations of PM_{10}. This agrees with the fact that it is the fine fraction of PMs that is most potently created in combustion processes, which are typical for residential heating in winter (We can even see that for year 2017 in Figure 7, the values for $PM_{2.5}$ and PM_{10} are the same; hence, all of the differences between the summer and winter concentrations of PMs can be attributed to the fine fraction). Further, the coarse fraction $PM_C = PM_{10} - PM_{2.5}$ therefore has slightly higher concentrations in summer than in winter. The PM_C is mostly connected to the dust processes, which are more prominent in summer compared to winter; hence, this is also consistent with the results.

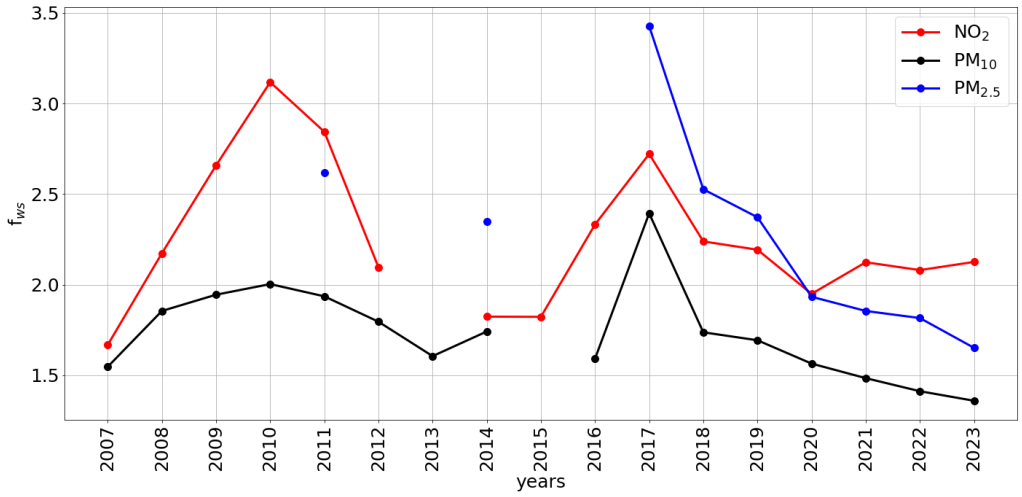

Figure 6. f_{ws} factor for station average of NO_2, PM_{10} and $PM_{2.5}$ concentrations.

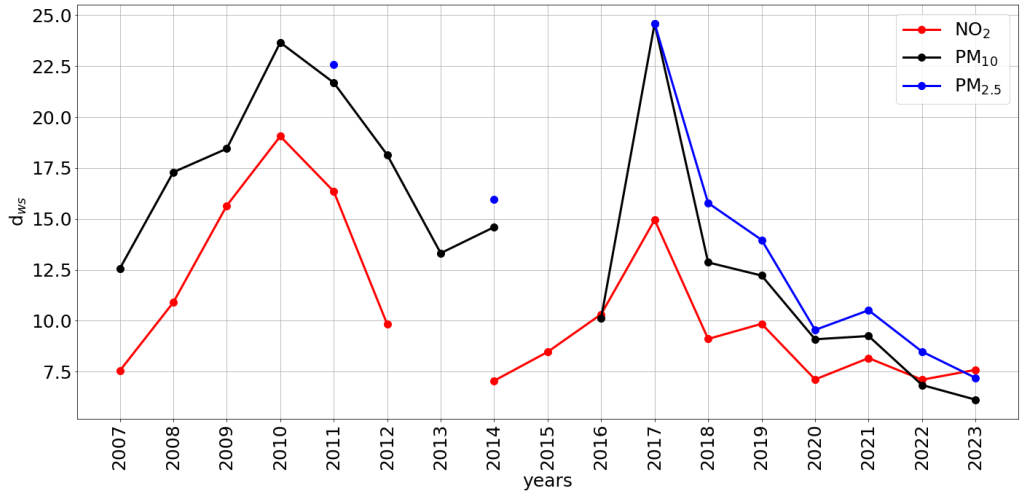

Figure 7. d_{ws} factor for station average of NO_2, PM_{10} and $PM_{2.5}$ concentrations.

3.2. Comparison of the Observed Mean Seasonal Factors with the Model CMAQ

The aim of this section is to assess if the model results are able to capture the measured seasonality. As described in Section 2.2, two full-year CMAQ model simulations for the years 2017 and 2023 with different configurations were used for the analysis. For these 2 years, the f_{ws} factors based on observations and model simulations are presented in Figure 8. The observed f_{ws} factors are the same as in Figure 6 for the respective years. The model f_{ws} factors were calculated as a mean of the f_{ws} factors for grid cells of the model in which the respective monitoring stations are situated.

From Figure 8, one can see that both measurements and models show that the winter concentrations are higher than the summer ($f_{ws} > 1$) for all the assumed pollutants. For NO_2 and $PM_{2.5}$ in 2017, the modelled f_{ws} is almost the same as the observed one. For the other cases, the modelled f_{ws} are higher than the measured ones by around 0.5 to 1. Both models and measurements show that the $PM_{2.5}$ f_{ws} is larger than for PM_{10}. For 2017, this difference is much more apparent for the observations, where the f_{ws} is larger by 1 for $PM_{2.5}$ compared to PM_{10}; for the model, the difference is only around 0.2. For 2023, the $PM_{2.5}$ f_{ws} is larger than the PM_{10} f_{ws} by around 0.3 for both model and observations. Both measurements and models also show that f_{ws} for PMs was substantially smaller in 2023 than in 2017. The observed f_{ws} for NO_2 was smaller in 2023 than in 2017, but the model shows a larger f_{ws} in 2023.

The difference between the winter and summer concentrations d_{ws}, computed from the same data as for f_{ws} in Figure 8, is presented in Figure 9. While in 2023, the modelled d_{ws} agrees well with the observations, the model was not able to capture the unusually large d_{ws} due to the very cold January in 2017, which resulted in large model BIAS for the winter, as explained in Section 2.4.

The difference between the observed d_{ws_o} and modelled d_{ws_m} can be expressed with the model bias as

$$d_{ws_o} - d_{ws_m} = \mathrm{BIAS}_s - \mathrm{BIAS}_w, \quad (3)$$

where the model bias is defined for winter as $\mathrm{BIAS}_w = \bar{c}_{w_m} - \bar{c}_{w_o}$ (similarly for summer). In our case, both summer and winter BIAS are negative. Hence, if d_{ws_o} is larger than d_{ws_m}, the left side of Equation (3) is positive and the $|\mathrm{BIAS}_w|$ must be larger than $|\mathrm{BIAS}_s|$. Applying this to the results in Figure 9, the $|\mathrm{BIAS}_w|$ in 2017 must be much higher than $|\mathrm{BIAS}_s|$ and for 2023 the BIAS_w and BIAS_s are comparable. This is also confirmed by the validation of the model in Section 2.4.

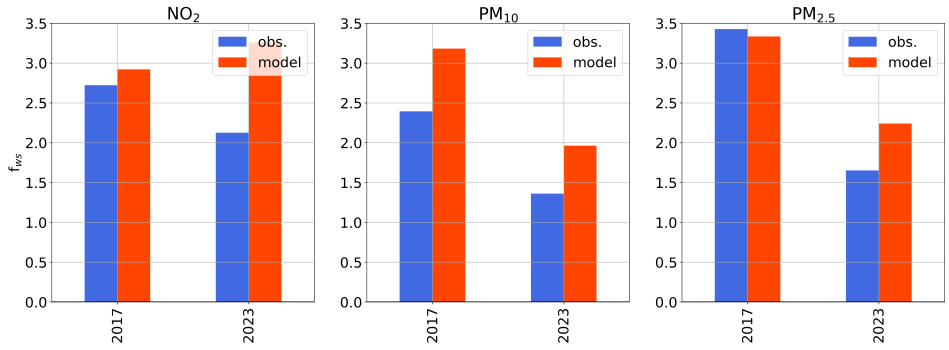

Figure 8. Average f_{ws} factor for NO_2, PM_{10} and $PM_{2.5}$ concentrations at the monitoring stations and corresponding model grid cells.

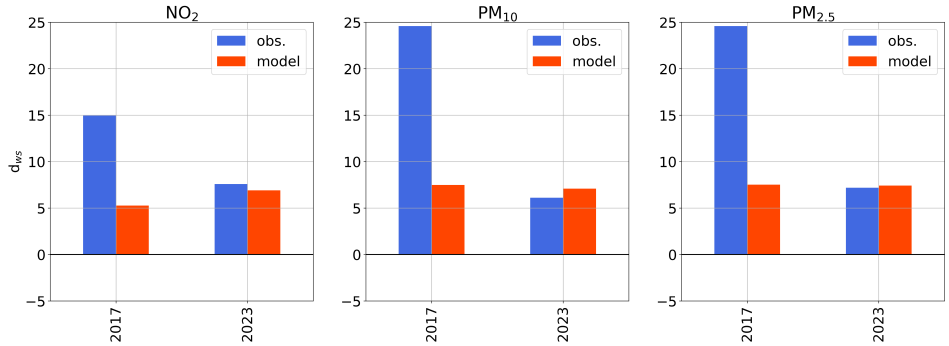

Figure 9. Average d_{ws} factor for NO_2, PM_{10} and $PM_{2.5}$ concentrations at the monitoring stations and corresponding model grid cells.

Comparing Figures 8 and 9, one can see that for 2023, the difference between the winter and summer concentrations d_{ws} is well captured by the model for all pollutants, but the ratio of winter to summer concentration f_{ws} is overestimated by the model. On the other hand, in the case of $PM_{2.5}$ and NO_2 in 2017, the modelled and observed f_{ws} agree well, despite the large disagreement in the case of d_{ws}. It can be shown that the model can predict the f_{ws} well in two cases. In the first case, both summer and winter BIAS are negligible in comparison to the observations. In the second case, the ratio between winter to summer BIAS is close to the observed ratio f_{ws_o}. These facts can be derived from the equation for the modelled f_{ws_m}

$$f_{ws_m} = \frac{\bar{c}_{w_o} + \mathrm{BIAS}_w}{\bar{c}_{s_o} + \mathrm{BIAS}_s}, \tag{4}$$

where $\bar{c}_{w_o}$ ($\bar{c}_{s_o}$) and BIAS_w (BIAS_s) are the observed mean winter (summer) concentrations and their modelled BIAS. Denoting the observed factor as $f_{ws_o} = \frac{\bar{c}_{w_o}}{\bar{c}_{s_o}}$, the following relations can be derived from Equation (4):

$$\begin{aligned} f_{ws_m} &= f_{ws_o} \Leftrightarrow \frac{\mathrm{BIAS}_w}{\mathrm{BIAS}_s} = f_{ws_o} \quad \text{for} \quad \mathrm{BIAS}_s \neq 0 \\ f_{ws_m} &> f_{ws_o} \Leftrightarrow \frac{\mathrm{BIAS}_w}{\mathrm{BIAS}_s} \gtrless f_{ws_o} \quad \text{for} \quad \mathrm{BIAS}_s \gtrless 0 \\ f_{ws_m} &< f_{ws_o} \Leftrightarrow \frac{\mathrm{BIAS}_w}{\mathrm{BIAS}_s} \lessgtr f_{ws_o} \quad \text{for} \quad \mathrm{BIAS}_s \gtrless 0. \end{aligned} \tag{5}$$

In the case of 2023, the model has a similar negative BIAS for both winter and summer periods, and therefore $\frac{\mathrm{BIAS}_w}{\mathrm{BIAS}_s} \approx 1$, which is less than f_{ws_o} for all pollutants in Figure 8. Equation (5) therefore implies that the model over-predicts the observed f_{ws} factors, as is confirmed in Figure 8. In this case, the model underestimates the summer concentrations proportionally more than the winter ones. In the case of 2017, a large difference between

the summer and winter BIAS was observed, but in the case of NO_2 and $PM_{2.5}$, the f_{ws} factor was predicted well. In this case, the Equation (5) implies that the ratio $\frac{\mathrm{BIAS}_w}{\mathrm{BIAS}_s} \approx f_{ws_o} = \frac{\bar{c}_{w_o}}{\bar{c}_{s_o}}$. In this case, the model BIAS grows proportionally to the concentrations.

3.3. Comparison of Observed Seasonal Factors with Model CMAQ at Individual Stations

The figures in this section show the average annual f_{ws} and d_{ws} for the individual monitoring stations for the years 2017 and 2023. The observed f_{ws} and d_{ws} are compared to the f_{ws} and d_{ws} computed from the corresponding grid cells of the model CMAQ. Figures 8 and 9 show the average of these figures for each pollutant for f_{ws} and d_{ws}, respectively. Further, the following figures show the station types, indicated by different colors of the background. Some stations have missing observed data for one of the displayed years. Appendix B contains figures with the mean f_{ws} and d_{ws} for the station types.

3.3.1. NO_2

Starting with Figure 10, which shows the f_{ws} for NO_2, we can see a large variety in f_{ws} among the individual stations and the 2 years, even within the stations of the same type. First looking at the observed f_{ws} (blue for 2017 and green for 2023), we can see that the T and I stations generally have smaller values of f_{ws} compared to the B stations. This is probably caused by the fact that these stations are positioned near large sources of NO_x (traffic and industry, respectively), which usually do not have a distinct seasonal profile. This is best seen for stations BA Trn. M., Trnava, or Presov, which all show f_{ws} factor close to 1. The NR Sturova is the only station showing f_{ws} smaller than 1, meaning this station had larger summer emissions compared to the winter ones. This can indicate a potential error of the NO_2 measurements in this station during 2023. On the other hand, the B stations are farther away from all emission sources; hence, they are affected by a combination of various emission sources from larger distances. The SB and UB stations are more affected by traffic, residential heating, and industry from settlements, while the RB stations are more affected by biogenic emissions and long-distance-transported concentrations, also called the concentration background. Out of the B stations, the smallest f_{ws} is observed at stations Chopok and Kojsovska H., which are both positioned at the top of a mountain, so they are almost unaffected by the emission sources and ground-level temperature inversions. The stations with the highest seasonality in the case of NO_2 seem to be the stations that are most affected by poor dispersion conditions during winter due to their position within a valley or stations that are most affected by residential heating (Jelsava, BB Zelena).

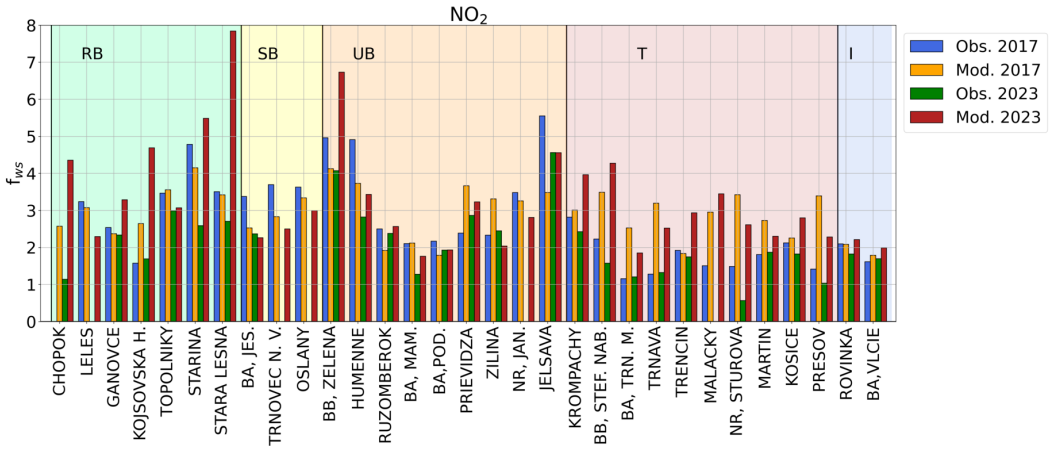

Figure 10. Average f_{ws} factor for NO_2 concentrations at the individual stations and corresponding model grid cells for the years 2017 and 2023.

The modelled f_{ws} for 2017 (yellow) does not distinguish well between the station types (apart from I stations with lower values of f_{ws}), as in the case of observations. This is more obvious for the mean f_{ws} for the station types, which is presented in Figure A1 in the

Appendix B. This most likely happens due to a rather large resolution of the model (4.7 km), which does not allow us to detect effects on a sub-grid scale, such as peaks in concentrations or effects of complex orography. The effect is the most visible for the T stations, where the observations consistently show smaller values while the model overestimates these values, and for RB stations, where the model matches the observed f_{ws} well for most stations. The overestimation for the T stations happens most likely due to their close vicinity to roads, where the influence of the traffic sector is predominant during the whole year compared to the other sectors, and hence, we do not observe large seasonal variations in concentrations at this type of station. Due to the large area of the model grid cell, the concentrations are also affected by other emission sectors apart from the traffic sector, which makes the seasonality of the model concentrations larger in comparison to the observations. In contrast, the RB stations are affected by a combination of many sources, whose concentrations are well mixed, which is much closer to the model output. For 2023 (red), the model significantly overestimates the observed f_{ws} for most RB and some UB stations, while it matches the observed f_{ws} well for most UB stations. For T stations, the model still consistently predicts higher values of f_{ws} than the observed ones, even though the model resolution has been significantly improved. Both models predicted the f_{ws} very well for the I stations. This is probably caused by the concentrations being higher in a larger vicinity around the industries and better accuracy of the emissions, since the industries are required to report them.

In Figure 11, we present the d_{ws} for NO_2. For 2017, we can see large differences between the observed values at the different station types. The smallest d_{ws} was observed at the RB stations and then the I stations; the SB and UB stations show similar results and for T stations, we see a couple of stations with the highest d_{ws} (BB, Stef. nab., Trencin, Kosice) and a few with very small d_{ws} (BA Trn. M., Trnava). We think that the stations with the high d_{ws} are the stations showing a larger influence of the residential heating on the surroundings, while the for the stations with low d_{ws}, the T is the main source of NO_x pollution. For 2023, the observed d_{ws} is much smaller than for 2017 at almost all stations, with values around 6 $\mu g \cdot m^{-3}$ for all station types, apart from RB stations with d_{ws} values around 3 $\mu g \cdot m^{-3}$. In comparison, the 2017 observations reached values around 17 $\mu g \cdot m^{-3}$ for SB, UB and T stations, around 6 $\mu g \cdot m^{-3}$ for RB stations and around 11 for I stations. For 2023, the d_{ws} factor is the largest at the UB stations; similar for SB, T and I stations; and the lowest for R stations. For the NR Sturova station, where the $f_{ws} < 1$, we can see a negative d_{ws}.

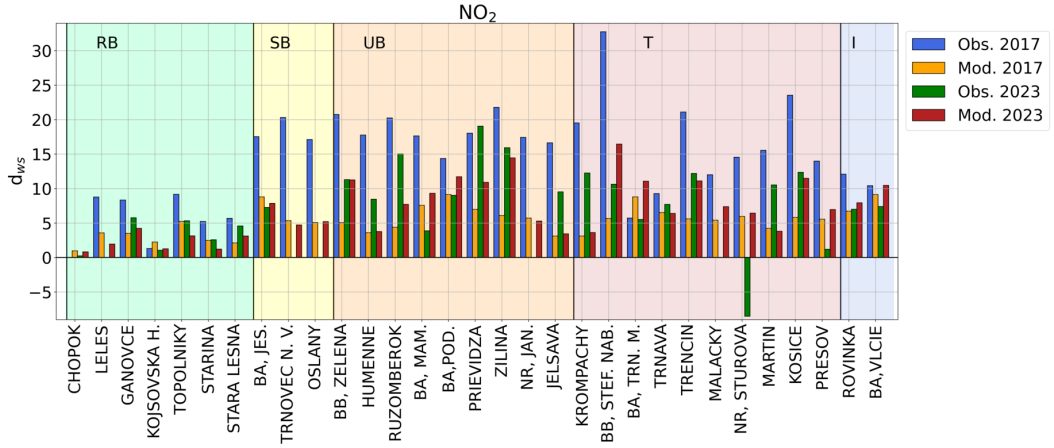

Figure 11. Average d_{ws} factor for NO_2 concentrations at the individual stations and corresponding model grid cells for the years 2017 and 2023.

By comparing the observed d_{ws} with the modelled values, we can see that although the model heavily underestimates the observed values of d_{ws} (mainly due to the large model bias in general), on average, the model predicts higher values of d_{ws} for places with higher observed d_{ws}. The underestimation of the model is much more apparent for 2017, due to unusually high observed d_{ws} and also likely due to the larger model resolution of

4.7 km. For 2023, the model matches the observations much better; however, for most of the stations, it either overestimates or underestimates the d_{ws}. For only about a third of the stations, the model's d_{ws} is close to the observed value. These differences are probably mainly caused by the resolution of the model and the spatio-temporal distribution of the NO_x emissions.

3.3.2. PM_{10}

The PM_{10} f_{ws} values for individual stations are presented in Figure 12. For the observed f_{ws}, we do not see major differences between the station types, although in general, the RB stations seem to have slightly lower values and the UB seem to have slightly higher values than the rest of the stations. The 2017 observed f_{ws} is again much larger, about twice the size of the 2023 f_{ws}, due to the very cold January of 2017. We can see that most R stations in 2023 have an $f_{ws} < 1$, indicating larger summertime concentrations. The highest f_{ws} was reached for both years at stations Ružomberok and Jelšava, which are strongly affected by the effects of residential heating.

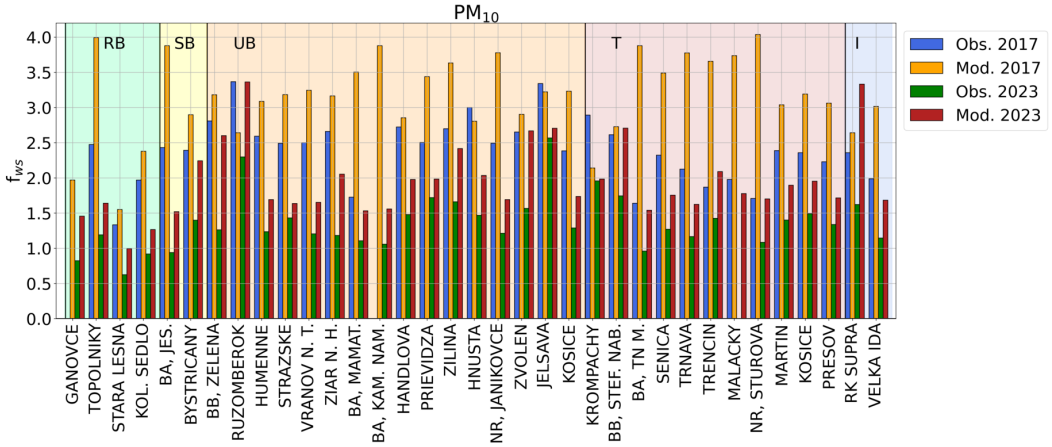

Figure 12. Average f_{ws} factor for PM_{10} concentrations at the individual stations and corresponding model grid cells for the years 2017 and 2023.

The 2017 simulation largely overestimates the observed f_{ws} at the majority of stations. This is likely due to the winter bias of the model being proportionally smaller as compared to the summer bias, as explained in Section 3.2. The overestimation is again the largest for T stations, due to the same reasons as in the case of NO_2. The 2023 simulation also overestimates the observed f_{ws} on majority of stations, but to a lesser extent, and correlates better with the observations. This is likely caused by the better resolution of the new model setup, which allows for better resolution of emissions, meteorology, and orography of the model. For the 2017 setup, the model values are spread over a larger area, so the model basically only represents the background and is not comparable to T stations.

The PM_{10} d_{ws} values for individual stations are presented in Figure 13. Looking at the observed values of d_{ws}, we can see the 2017 observations having as much as 4 times larger values than 2023. For majority of the stations, the 2017 d_{ws} shows values above 20 $\mu g \cdot m^{-3}$, while for 2023, most stations show d_{ws} under 10 $\mu g \cdot m^{-3}$. For both years, the highest d_{ws} was observed for stations Ružomberok and Jelšava, which also have the largest f_{ws} for PM_{10}. We can now see five stations with negative values of d_{ws} for 2017, and a few other stations with very small positive values of d_{ws}. The d_{ws} values are the smallest for the RB and SB stations and similar for other station types.

For the majority of stations, there are small differences between d_{ws} of the two model simulations; however, the 2023 simulation matches the observed d_{ws} much better. While the 2017 simulation strongly underestimates the observations, the 2023 d_{ws} mostly slightly overestimates the observations. For both model simulations, we do not see clear patterns

between the d_{ws} values of different station types, other than the RB stations having the smallest values.

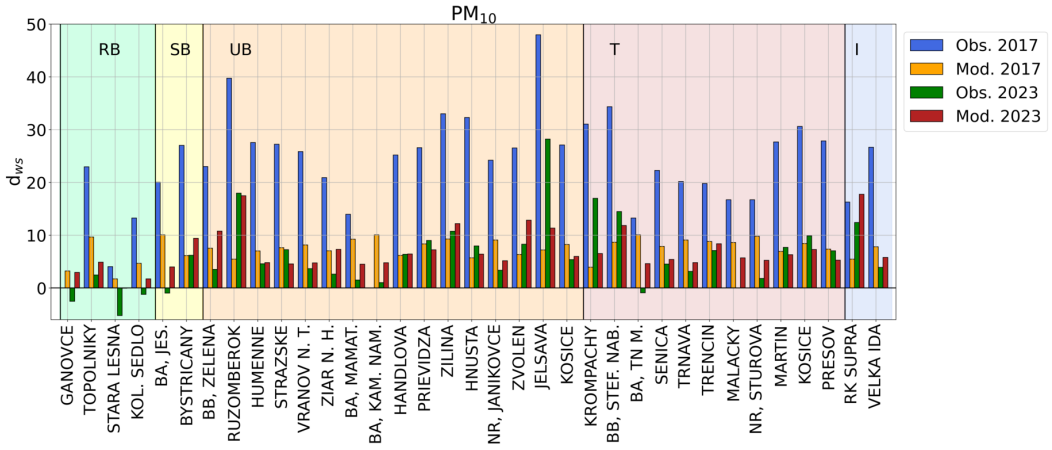

Figure 13. Average d_{ws} factor for PM_{10} concentrations at the individual stations and corresponding model grid cells for the years 2017 and 2023.

3.3.3. $PM_{2.5}$

For the f_{ws} of $PM_{2.5}$ (Figure 14), we can see that the observed values are considerably higher than the PM_{10} for most stations. The difference is more apparent for 2017. Further, for $PM_{2.5}$, we can see larger differences between the station types, namely, most B stations have larger observed f_{ws} compared to T and I stations. We can also see much higher values of f_{ws} for the RB stations for $PM_{2.5}$. These differences can be attributed to the largest seasonality of the $PM_{2.5}$ originating from residential heating, which mostly affects the B stations. The T and I stations are less affected due to the larger influence of the traffic and industrial sources in their vicinity. Stations with the largest observed f_{ws} for both years are Hnusta, Jelsava, Zvolen, BB Stef. nab. and Ruzomberok, which are the stations that are mostly affected by residential heating.

For the B stations, the modeled f_{ws} for both years matches the observations better than for PM_{10}. The 2017 simulation now mostly underestimates the observed f_{ws} for the B stations, while for PM_{10}, the model overestimated the observed f_{ws}. For the T stations, the 2017 simulation strongly overestimates the observed f_{ws}, while the 2023 simulation matches the T stations more closely. This can be again attributed to the fact that the model resolution for 2017 is 4.7 km, so its concentration results are comparable to background concentrations, where the emissions from the whole grid cell are well mixed. The finer resolution of the 2023 simulation again improved the accuracy of the model.

Finally, the d_{ws} for $PM_{2.5}$ at the individual stations is presented in Figure 15. For the majority of stations, the d_{ws} for $PM_{2.5}$ is only slightly smaller than for PM_{10}. This can be attributed to the fact that the majority of the seasonal variation in PM_{10} can be attributed to $PM_{2.5}$, as shown previously. In other words, it is the increase in $PM_{2.5}$ during the winter which also causes the increase in PM_{10} for the majority of the stations. The only exception is the T station Trencin in 2017, where the d_{ws} was around 20 $\mu g \cdot m^{-3}$ for PM_{10} but only around 2 $\mu g \cdot m^{-3}$ for $PM_{2.5}$. Such a difference in the d_{ws} for PM_{10} and $PM_{2.5}$ can indicate the potential error of the $PM_{2.5}$ measurements due to malfunction of the measuring device. Upon further inspection of data in this particular case, it was found that the measurements at the Trencin station were systematically underestimated in comparison to the other stations from the beginning of the year 2017 until May. While the operator did not notice any extraordinary behaviour at the time of the measurements, this systematic underestimation became evident with our analysis of the seasonality. This underestimation is most likely caused by the incorrect calibration of the measuring device.

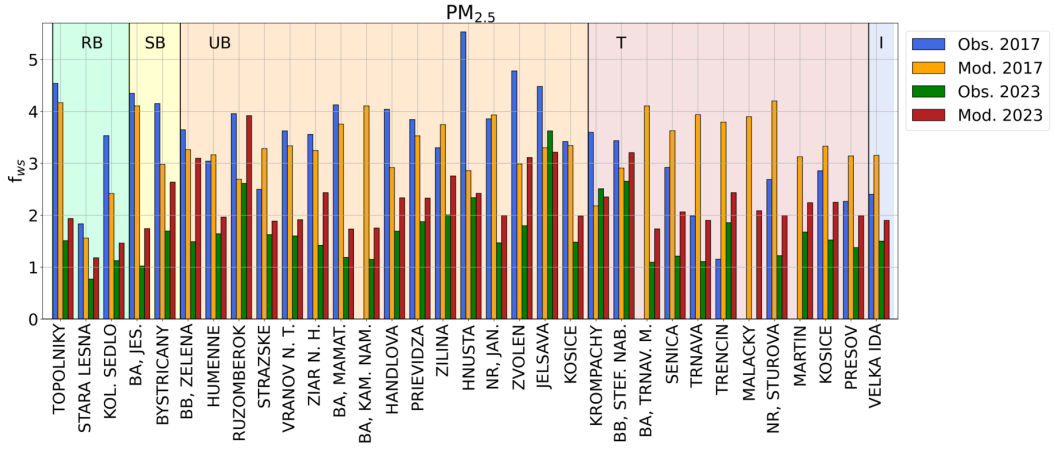

Figure 14. Average f_{ws} factor for $PM_{2.5}$ concentrations at the individual stations and corresponding model grid cells for the years 2017 and 2021.

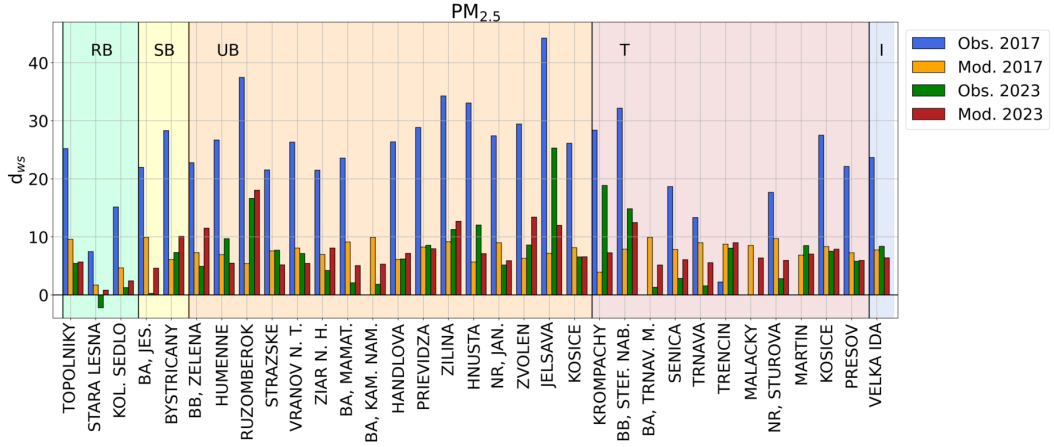

Figure 15. Average d_{ws} factor for the $PM_{2.5}$ concentrations at the individual stations and corresponding model grid cells for the years 2017 and 2021.

4. Discussion

Meteorological conditions affect the dispersion of pollutants throughout the year and, together with seasonal emissions, create patterns in concentrations of pollutants. In Slovakia, we observe the largest differences between the concentrations in winter vs. in summer. In winter, emissions from residential heating combined with poor dispersion conditions often lead to high concentrations of pollutants, primarily $PM_{2.5}$ and PM_{10}. In summer, the residential heating emissions are nearly negligible, and the dispersion conditions are usually favourable, which leads to overall lower concentrations of most pollutants. However, due to climate change, the character of seasons in Slovakia is slowly changing and we now observe milder winters, which are associated with better dispersion conditions.

To quantitatively evaluate the seasonality of AQ in Slovakia, we introduced two simple factors, which use mean summer (June, July, August) and winter (December, January, February) concentrations: the ratio of winter to summer concentrations f_{ws} and the difference between the winter and summer concentrations d_{ws}. The seasonality of AQ was analysed for PM_{10}, $PM_{2.5}$ and NO_2. There have been no prior studies analysing the seasonal changes in the AQ and their trends in Slovakia. The main goals of the paper were to analyse the observed AQ through the introduced factors, to observe trends in the seasonal factors, and to compare the observed seasonality with two model simulations with the model CMAQ.

For PMs, the national mean f_{ws} gradually declined during the studied period. This is a consequence of a decrease in winter concentrations, while the summer concentrations have been nearly constant since 2016. The winter PM concentrations have been decreasing due to milder winters, which, apart from better dispersion conditions, implies lower heating

demand. Further, new buildings and the thermal insulation of old houses might have also lead to lower emissions. Since the emissions of PMs have not been changing much since 2014 [22], we consider the milder winters with better dispersion conditions to be the main reason for the lower winter concentrations of PMs.

It was shown that the f_{ws} factor is generally higher for $PM_{2.5}$ compared to PM_{10}. The reason is that the emissions of $PM_{2.5}$ are mostly emitted during winter, while there are additional emission sources of coarse fraction of PM in summer, i.e., Saharan dust, wind blowing over bare soil lands, agriculture, and construction works and road dust resuspension. For some RB stations, larger concentrations of PM (especially PM_{10}) were observed in summer than in winter. As the winter concentrations are on a decline, the summer sources of PM emissions start to play a more important role for the AQ than in the past. Nevertheless, many areas in Slovakia still experience very poor AQ conditions due to high PM concentrations during winter.

The f_{ws} for NO_2 has been rather constant since 2018 due to both winter and summer concentrations decreasing at a similar rate. The main NO_2 emission sources are traffic and industry, which do not have a significant annual variability. The local heating, which has a strong seasonal variability, only comprises a small portion of total NO_2 emissions. The decrease in NO_2 concentrations in recent years can be mostly attributed to the gradual decrease in the traffic emissions [22]. Even though the emissions of NO_2 do not have a significant annual profile, the f_{ws} for NO_2 is generally higher than for PM_{10}, and for the last couple of years even for $PM_{2.5}$. Therefore, we assume that the NO_2 seasonality is mostly caused by the seasonal changes in dispersion and meteorological conditions and less by seasonal emission changes.

The comparison of the modelled f_{ws} and d_{ws} to the observed values showed the importance of understanding the BIAS of the model and its effect on the computed factors. Our results show that the f_{ws} factor is very sensitive to the ratio of winter to summer BIAS of the model, and a small change in this ratio caused a disagreement between the model and the observed f_{ws}. We have shown that the modelled f_{ws} matches the observations if the BIAS of the model is negligible, or the ratio of model winter to summer BIAS is equal to the ratio of the observed winter to summer concentrations. Therefore, the parameter f_{ws} can be used to test the proportionality of the model BIAS to the observed concentrations. This is a reasonable assumption for the model results, since it implies that the BIAS of the model grows proportionally with the predicted values. When the ratio of the model BIAS is different from the observed seasonality, it might imply that the model emissions are not well distributed in space and time or that the model is not capable to effectively predict certain meteorological conditions that might only occur during winter or summer. An equal BIAS for summer and winter implies that the model underestimates the lower summer concentrations proportionally more (by a higher relative percentage) than the winter ones, and hence the model is more biased for the summer. The d_{ws} might therefore be a better factor to observe the capacity of the model to predict the seasonality, since it provides a direct difference between the winter and summer values.

For the 2023 simulation, the modelled d_{ws} agrees with the observation for all pollutants for the national mean. The model overestimated f_{ws} since the model's summer and winter biases were similar. In the case of the 2017 simulation, the model was not able to capture the observed unusually high concentrations during the extremely cold January and therefore was not able to capture the observed high values of d_{ws}. On the other hand, the f_{ws} factor was predicted quite well, which shows that the ratio of winter to summer BIAS was proportional to the ratio of the observed winter to summer concentrations.

Our analysis of the modelled seasonality has only been carried out for the years 2017 and 2023, since these were the only available simulations which covered a whole year. Since September 2023, model CMAQ has been running operationally at SHMU to provide AQ forecasts for Central Europe. Therefore, more modelled data will be available in the future and additional tests of modelled seasonality could be carried out. Seasonal analysis of the model results might also lead to future improvements to the model. For example,

the analysis of the size of the model bias throughout the year might indicate different deficiencies of the model for different seasons. Worse performance of the model for some of the seasons might imply that the model does not have the correct emission inputs for that time of the year (emissions are too low, or temporal emission profiles do not reflect real societal patterns well), some meteorological phenomena might not be well resolved and computed in the model, or the chemical mechanism of the model is somehow skewed depending on meteorological conditions. However, a much more detailed analysis than ours would be required to correctly assess such causes.

In the future, we are planning to test the seasonality of the model using emission inputs with various time profiles in order to evaluate the impact of seasonal emissions and meteorological changes on model concentrations. For example, variation in concentrations computed using constant emission profiles would show the variation caused by meteorological conditions and chemical reactions in the model. Comparing such a simulation with one with varying emission profiles would allow us to evaluate the impact of the time variation of the emissions on the resulting concentrations.

There have been several studies analysing seasonal changes in the air quality using data from satellites. The seasonality of surface concentrations of six pollutants over China was studied based on data from the Geostationary Environment Monitoring Spectrometer (GEMS) [54], and the GEMS NO_2 data have also been compared to the hourly ground measurements of NO_2 [55]. Changes in monthly averages of tropospheric NO_2 vertical column density were analysed with the Ozone Monitoring Instrument (OMI) [56]. The satellite data on aerosol optical depth from the Sea and Land Surface Temperature Radiometer were used in combination with the Moderate Resolution Imaging Spectroradiometer to obtain surface $PM_{2.5}$ concentrations [57]. These, and other satellites such as Sentinel-5P TROPOMI [58], could be used for future analysis of the seasonality of AQ in Slovakia to provide additional information and for comparison with observed and modelled data.

5. Conclusions

Based on observations from monitoring stations in Slovakia, it was found that the mean annual concentrations of PM_{10} and $PM_{2.5}$ steadily decreased from 2017 to 2023. The decrease is the most prominent during the winter season (JFD). On the other hand, the concentrations were almost constant during the summer season (JJA). Over the past four years, the mean winter PM_{10} ($PM_{2.5}$) concentrations were around 1.5 (1.9) times higher than the summer ones, which corresponds to an increase of around 8 (9) $\mu g \cdot m^{-3}$. Since the PM concentrations during the winter season are mostly affected by the emissions from local heating, which are negligible in summer, these emissions together with worse dispersion conditions in winter are the main cause of the winter increase in concentrations. The World Health Organization (WHO) guidelines [59] state that the annual average exposure of $PM_{2.5}$ and PM_{10} should not exceed 5 $\mu g \cdot m^{-3}$ and 15 $\mu g \cdot m^{-3}$, respectively. In recent years, the average summer concentrations of $PM_{2.5}$ and PM_{10} in Slovakia have been around 11 $\mu g \cdot m^{-3}$ and 17 $\mu g \cdot m^{-3}$, so it is evident that the air quality measures concerning just the local heating alone are not sufficient to satisfy the WHO annual air quality guidelines, despite significantly helping to reduce the concentrations during high-emission episodes and the number of daily exceedances. Therefore, measures concerning other sources of PM, which affect the summer concentrations, are also needed.

In the case of NO_2, both mean summer and winter concentrations have been slightly decreasing since 2017. Over the past four years, the mean winter NO_2 concentrations have been around 2.1 times higher than the summer ones, which corresponds to an increase of around 7.5 $\mu g \cdot m^{-3}$. For the same period, the annual average NO_2 concentrations have been a little below 15 $\mu g \cdot m^{-3}$, while the WHO annual air quality guidelines' level for NO_2 is 10 $\mu g \cdot m^{-3}$. It is expected, that the mean NO_2 exposure for people in Slovakia will satisfy the WHO annual air quality guidelines level in the upcoming years due to the development of electromobility, although some hotspots near the roads will still exist.

In this work, the seasonality of AQ was also analysed for model simulations with the chemical-transport model CMAQ. The purpose of this analysis was to obtain seasonal patterns of AQ in areas not covered by the measuring sites and to analyse the capacity of the model to capture the observed seasonality. The results of two model simulations for the years 2017 and 2023 were analysed and compared with measurements from the monitoring stations. While for 2017, the model results did not match the observed seasonality well due to unexpectedly high winter concentrations in 2017, for 2023, with a milder winter and finer resolution of the model, the modelled seasonality matched the observed much more closely for most monitoring stations.

Author Contributions: Conceptualization, T.Š. and D.Š.; methodology, D.Š. and T.Š.; validation, T.Š.; resources, T.Š.; data curation, T.Š. and D.Š.; writing—original draft preparation, T.Š.; writing—review and editing, D.Š.; visualization, T.Š.; supervision, D.Š. All authors have read and agreed to the published version of the manuscript.

Funding: This research received no external funding.

Institutional Review Board Statement: Not applicable.

Informed Consent Statement: Not applicable.

Data Availability Statement: The raw data supporting the conclusions of this article will be made available by the authors on request.

Conflicts of Interest: The authors declare no conflicts of interest.

Abbreviations

The following abbreviations are used in this manuscript:

AQ	Air quality
I	Industrial
NMSKO	National air-quality monitoring network
NO	Nitric oxide
NO_2	Nitrogen dioxide
NO_x	Nitrogen oxides
PM	particulate matter
PM_{10}	PM with diameter smaller than 10 µm
$PM_{2.5}$	PM with diameter smaller than 2.5 µm
PMs	PM_{10} + $PM_{2.5}$, both fractions of PM
PM_C	$PM_{10} - PM_{2.5}$, coarse fraction of PM_{10}
RB	Rural background
SB	Suburban background
SHMU	Slovak hydrometeorological institute
T	Traffic
UB	Urban background
WHO	World Health Organization

Appendix A. Air Quality Monitoring Sites

Table A1. Monitoring stations used in the analysis. Station types: B—background, T—traffic, I—industrial; Locations: R—rural, U—urban, S—suburban. The short names are used in figures. Elevation is in metres above the mean sea level. The 1/0 indicates whether the station measures/does not measure the given pollutant. The position of stations in Slovakia, labelled by station number N, can be seen in Figure 1.

N	Name/Short Name	Lat	Lon	Elevation	Location/Type	PM_{10}	$PM_{2.5}$	NO_2
1	Bratislava, Jeséniova/BA, JES.	48.167952	17.106209	287	S/B	1	1	1
2	Chopok/CHOPOK	48.94362	19.589236	1990	R/B	0	0	1
3	Gánovce/GANOVCE	49.034601	20.322844	706	R/B	1	0	1
4	Kojšovská Hoľa/KOJSOVSKA H.	48.782875	20.987112	1232	R/B	1	0	1
5	Bratislava, Mamateyova/BA, MAM.	48.124692	17.1254	138	U/B	1	1	1
6	Bratislava, Trnavské Mýto/BA, TRN. M.	48.158359	17.128891	136	U/T	1	1	1
7	Bratislava, Kam. Nám./BA, KAM. NAM.	48.14467	17.113543	139	U/B	1	1	0
8	Senica / SENICA	48.680681	17.36311	212	U/T	1	1	0
9	Trnava, Kollárova/TRNAVA	48.371385	17.584926	152	U/T	1	1	1
10	Trnovec nad Váhom/TRNOVEC N. V.	48.15	17.9286	114	S/B	1	0	1
11	Trenčín, Hasičská/TRENCIN	48.896419	18.04124	214	U/T	1	1	1
12	Oslany (SE Nováky)/OSLANY	48.6333	18.47	228	S/B	1	0	1
13	Malacky, Mierové nám./MALACKY	48.436843	17.019052	162	U/T	1	1	1
14	Nitra, Janíkovce/NR, JAN.	48.283059	18.140716	149	S/B	1	1	1
15	Nitra, Štúrova/NR, STUROVA	48.309436	18.07687	143	U/T	1	1	1
16	Banská Bystrica, Štef. náb./BB, STEF. NAB.	48.73511	19.154985	346	U/T	1	1	1
17	Banská Bystrica, Zelená/BB, ZELENA	48.733486	19.115325	425	U/B	1	1	1
18	Ružomberok (SUPRA SCP)/RK SUPRA	49.0786	19.32	478	U/I	1	0	0
19	Ružomberok, Riadok/RUZOMBEROK	49.079025	19.302536	475	U/B	1	1	1
20	Žiar nad Hronom, Jil./ZIAR N. H.	48.59959	18.842841	296	U/B	1	1	0
21	Bystričany, Rozvodňa (SSE)/BYSTRICANY	48.666957	18.514107	261	S/B	1	1	0
22	Handlová, Mor. Cesta/HANDLOVA	48.733096	18.756472	448	U/B	1	1	0
23	Prievidza, Malonecpalská/PRIEVIDZA	48.782641	18.628071	276	U/B	1	1	1
24	Žilina, Obežná/ZILINA	49.21147	18.771289	356	U/B	1	1	1
25	Hnúšťa, Hlavná/HNUSTA	48.583789	19.951648	320	U/B	1	1	0
26	Zvolen, J. Alexyho/ZVOLEN	48.558198	19.156881	321	U/B	1	1	0
27	Martin, Jesenského/MARTIN	49.05963	18.921378	383	U/T	1	1	1
28	Jelšava, Jesenského/JELSAVA	48.631194	20.240498	289	U/B	1	1	1
29	Košice, Štefánikova/KOSICE, ST.	48.72631	21.258902	209	U/T	1	1	1
30	Veľká Ida, Letná/VELKA IDA	48.592119	21.1752	209	S/I	1	1	0
31	Košice, Amurská/KOSICE, AM.	48.690223	21.285495	201	U/B	1	1	0
32	Prešov, Arm. Gen. L. Svo./PRESOV	48.992475	21.266767	252	U/T	1	1	1
33	Krompachy, SNP/KROMPACHY	48.915658	20.873901	372	U/T	1	1	1
34	Leles (SE Vojany)/LELES	48.4628	22.0231	100	R/B	1	0	1
35	Humenné, Nám. Slobody/HUMENNE	48.930897	21.913688	160	U/B	1	1	1
36	Strážske, Mierová/STRAZSKE	48.874013	21.837536	133	U/B	1	1	0
37	Vranov nad Topľou/VRANOV N.T.	48.886367	21.68758	133	U/B	1	1	0
38	Topoľníky/TOPOLNIKY	47.959423	17.860238	113	R/B	1	1	1
39	Starina/STARINA	49.042734	22.260012	345	R/B	0	0	1
40	Stará Lesná/STARA LESNA	49.151384	20.289529	808	R/B	1	1	1
41	Kolonické Sedlo/KOL. SEDLO	48.934886	22.273772	431	R/B	1	1	0
42	Rovinka (Slovnaft)/ROVINKA	48.104	17.2278	133	S/I	1	1	1
43	BA, Pod. Bisk. (Slovnaft)/BA, POD.	48.1347	17.2056	132	U/B	1	1	1
44	BA, Vlčie Hrdlo (Slovnaft)/BA, VLCIE	48.1333	17.1694	134	S/I	1	0	1

Appendix B. Mean Seasonal Factors for Station Types

The following figures show the f_{ws} and d_{ws} factors shown in Figures 10–15, averaged for the station types. These figures provide a good picture of the general trends between the station types; however, they are skewed by the small number of stations and some missing observation data, mainly for the SB and I stations. Therefore, the mean values

should serve as a guide, and for a full picture, we recommend analysing the values at the individual stations.

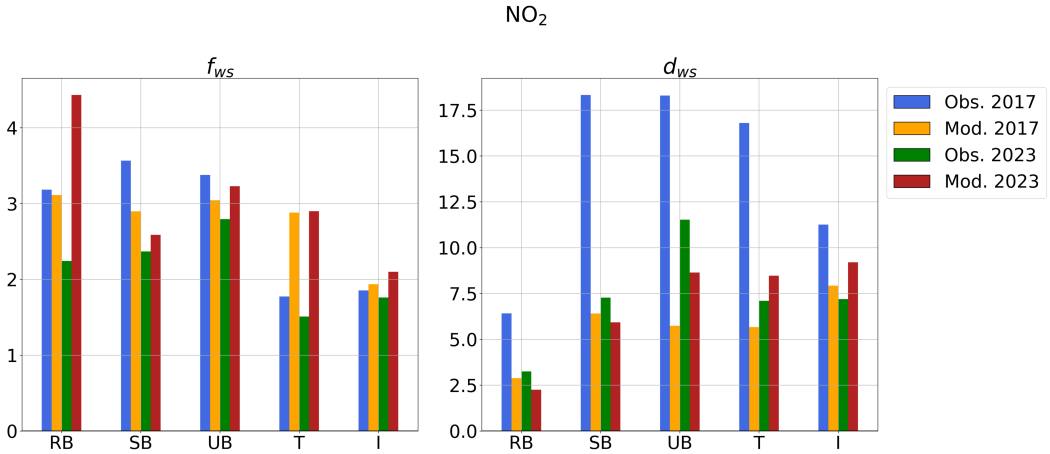

Figure A1. Average f_{ws} and d_{ws} factors for NO_2 concentrations for the station types and corresponding model grid cells for the years 2017 and 2023.

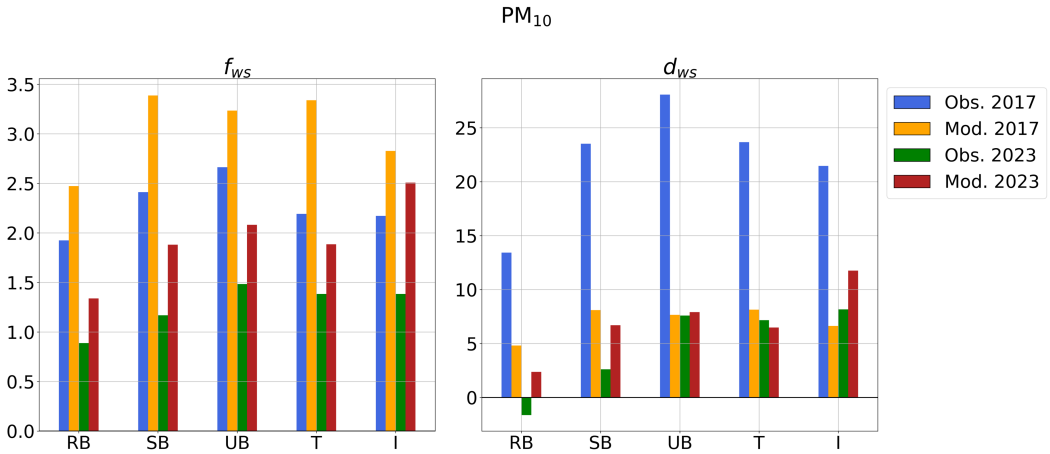

Figure A2. Average f_{ws} and d_{ws} factors for PM_{10} concentrations for the station types and corresponding model grid cells for the years 2017 and 2023.

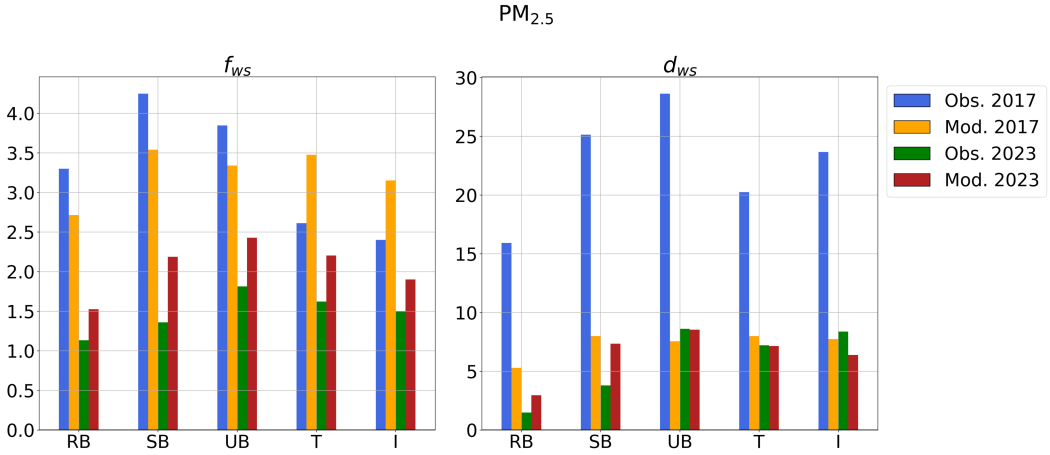

Figure A3. Average f_{ws} and d_{ws} factors for $PM_{2.5}$ concentrations for the station types and corresponding model grid cells for the years 2017 and 2023.

References

1. Fowler, D.; Brimblecombe, P.; Burrows, J.; Heal, M.R.; Grennfelt, P.; Stevenson, D.S.; Jowett, A.; Nemitz, E.; Coyle, M.; Liu, X; et al. A chronology of global air quality. *Philos. Trans. R. Soc. A* **2020**, *378*, 20190314. [CrossRef] [PubMed]
2. World Health Organization. *Ambient Air Pollution: A Global Assessment of Exposure and Burden of Disease*; World Health Organization: Geneva, Switzerland, 2016. Available online: https://iris.who.int/handle/10665/250141 (accessed on 30 August 2024).
3. Thangavel, P.; Park, D.; Lee, Y.-C. Recent Insights into Particulate Matter (PM2.5)-Mediated Toxicity in Humans: An Overview. *Int. J. Environ. Res. Public Health* **2022**, *19*, 7511. [CrossRef] [PubMed]
4. Kyung, S.; Jeong, S. Particulate-Matter Related Respiratory Diseases. *Tuberc. Respir. Dis.* **2020**, *83*. [CrossRef] [PubMed]
5. Holm, S.M.; Balmes, J.R. Systematic Review of Ozone Effects on Human Lung Function, 2013 Through 2020. *Chest* **2022**, *161*, 190–201. [CrossRef] [PubMed]
6. Brender, J.D. Human Health Effects of Exposure to Nitrate, Nitrite, and Nitrogen Dioxide. In *Just Enough Nitrogen*; Sutton, M.A., Ed.; Springer: Cham, Switzerland, 2020. [CrossRef]
7. Kowalska, M.; Skrzypek, M.; Kowalski, M.; Cyrys, J. Effect of NOx and NO2 Concentration Increase in Ambient Air to Daily Bronchitis and Asthma Exacerbation, Silesian Voivodeship in Poland. *Int. J. Environ. Res. Public Health* **2020**, *17*, 754. [CrossRef]
8. EEA. Europe's Air Quality Status 2023, Permalink (May 31, 2023 version). Available online: https://www.eea.europa.eu/publications/europes-air-quality-status-2023 (accessed on 28 March 2024).
9. Zhang, A.; Xia, C.; Li, W. Exploring the effects of 3D urban form on urban air quality: Evidence from fifteen megacities in China. *Sustain. Cities Soc.* **2022**, *78*, 103649. [CrossRef]
10. Wang, L.; Niu, D.; Fan, H.; Long, X. Urban configuration and $PM_{2.5}$ concentrations: Evidence from 330 Chinese cities. *Environ. Int.* **2022**, *161*, 107129. [CrossRef]
11. Shelton, S.; Liyanage, G.; Jayasekara, S.; Pushpawela, B.; Rathnayake, U.; Jayasundara, A.; Jayasooriya, L.D. Seasonal variability of air pollutants and their relationships to meteorological parameters in an urban environment. *Adv. Meteorol.* **2022**, *2022*, 5628911. [CrossRef]
12. Bodor, Z.; Bodor, K.; Keresztesi, Á.; Szép, R. Major air pollutants seasonal variation analysis and long-range transport of PM_{10} in an urban environment with specific climate condition in Transylvania (Romania). *Environ. Sci. Pollut. Res.* **2020**, *27*, 38181–38199. [CrossRef]
13. Liu, Y.; Zhou, Y.; Lu, J. Exploring the relationship between air pollution and meteorological conditions in China under environmental governance. *Sci. Rep.* **2020**, *10*, 14518. [CrossRef]
14. Manju, A.; Kalaiselvi, K.; Dhananjayan, V.; Palanivel, M.; Banupriya, G.S.; Vidhya, M.H.; Panjakumar, K.; Ravichandran, B. Spatio-seasonal variation in ambient air pollutants and influence of meteorological factors in Coimbatore, Southern India. *Air Qual. Atmos Health* **2018**, *11*, 1179–1189. [CrossRef]
15. Zareba, M.; Weglinska, E.; Danek, T. Air pollution seasons in urban moderate climate areas through big data analytics. *Sci. Rep.* **2024**, *14*, 3058. [CrossRef] [PubMed]
16. Dobson, R.; Siddiqi, K.; Ferdous, T.; Huque, R.; Lesosky, M.; Balmes, J.; Semple, S. Diurnal variability of fine-particulate pollution concentrations: data from 14 low- and middle-income countries. *Int. J. Tuberc. Lung Dis.* **2021**, *25*, 206–214. [CrossRef] [PubMed]
17. Soleimanpour, M.; Alizadeh, O.; Sabetghadam, S. Analysis of diurnal to seasonal variations and trends in air pollution potential in an urban area. *Sci. Rep.* **2023**, *13*, 21065. [CrossRef]
18. Pérez, I.A.; García, M.Á.; Sánchez, M.L.; Pardo, N.; Fernández-Duque, B. Key Points in Air Pollution Meteorology. *Int. J. Environ. Res. Public Health* **2020**, *17*, 8349. [CrossRef]
19. Mohtar, A.A.A.; Latif, M.T.; Baharudin, N.H.; Ahamad, F.; Chung, J.X.; Othman, M.; Juneng, L. Variation of major air pollutants in different seasonal conditions in an urban environment in Malaysia. *Geosci. Lett.* **2018**, *5*, 21. [CrossRef]
20. US EPA Office of Research and Development. *Zenodo*, CMAQ (5.3.3); US EPA: Washington, DC, USA, 2021. [CrossRef]
21. Štefánik, D.; Šedivá, T.; Krajčovičová, J.; Beňo, J.; Matejovičová, J. Operational air quality forecast for central Europe. In Proceedings of the 22nd International Conference on Harmonisation within Atmospheric Dispersion Modelling for Regulatory Purposes, Tartu, Estonia, 10–14 June 2024.
22. Slovak Hydrometeorological Institute with Ministry of Environment of the Slovak Republic. Informative Inventory Report 2023, Submission under the CLRTAP and NECD, Slovak Republic. 2023. Available online: https://oeab.shmu.sk/app/cmsFile.php?disposition=i&ID=209%27,%20%27SK_IIR_2023_v2%27 (accessed on 19 August 2024).
23. Krajčovičová, K.; Kocunová, Z. *Kvalita ovzdušia-príručka pre okresné úrady v oblasti ochrany ovzdušia (Air Quality—A Manual for District Offices for Air Protection Purposes)*; Ministry of Environment of the Slovak Republic, Slovak Environment Agency: Banská Bystrica, Slovakia, 2023; ISBN: 978-80-8213-124-9. Available online: https://www.enviroportal.sk/dokument/f/kvalita-ovzdusia.pdf (accessed on 20 August 2024).
24. Slovenský Hydrometeorologický ústav. Správa o Kvalite Ovzdušia v Slovenskej Republik—2019 (Air quality report for Slovakia-2019). 2020. Available online: www.shmu.sk/File/oko/rocenky/2019_Sprava_o_KO_v_SR%20v3.pdf (accessed on 20 August 2024).
25. Šťastný, P.; Sternová, Z.; Lapin, M. Dôsledky zmeny klímy na vykurovanie (Climate Change Impacts on Heating). *Život. Prostr.* **2004**, *38*, 250–256.
26. United States Environmental Protection Agency (EPA). Nitrogen Oxides (NO_x), Why and How They Are Controlled. Technical Bulletin; EPA 456/F-99-006R; Office of Air Quality Planning and Standards, Research Triangle Park. 1999. Available online: https://www3.epa.gov/ttn/catc/dir1/fnoxdoc.pdf (accessed on 22 August 2024).

27. Seinfeld, J.H.; Pandis, S.N. *Atmospheric Chemistry and Physics: From Air Pollution to Climate Change*, 2nd ed.; John Wiley & Sons, Inc.: Hoboken, NJ, USA, 2006; pp. 33–38.
28. US EPA Office of Research and Development. *Zenodo*, CMAQv4.7.1 (4.7.1); US EPA: Washington, DC, USA, 2010. [CrossRef]
29. Yarwood, G.; Rao, S.; Yocke, M.; Whitten, G.Z. Updates to the Carbon Bond Chemical Mechanism: CB05, Final Report to the US EPA RT-040067. (Technical Report), 2005. Available online: https://www.camx.com/Files/CB05_Final_Report_120805.pdf (accessed on 7 October 2024).
30. Binkowski, F.S. Models-3 Community Multiscale Air Quality (CMAQ) model aerosol component, 1. Model description. *Geophys. Res.* **2003**, *108*, 4183. [CrossRef]
31. Skamarock, W.C.; Klemp, J.B.; Dudhia, J.; Gill, D.O.; Barker, D.M.; Duda, M.G.; Huang, X.Y.; Wang, W.; Powers, J.G. *A Description of the Advanced Research WRF Version 3*; Note NCAR/TN-475+STR; National Center for Atmospheric Research: Boulder, CO, USA, 2008. .. [CrossRef]
32. Dou, X.; Yu, S.; Li, J.; Sun, Y.; Song, Z.; Yao, N.; Li, P. The WRF-CMAQ Simulation of a Complex Pollution Episode with High-Level O_3 and $PM_{2.5}$ over the North China Plain: Pollution Characteristics and Causes. *Atmosphere* **2024**, *15*, 198. [CrossRef]
33. Zhang, S.; Zhang, Z.; Li, Y.; Du, X.; Qu, L.; Tang, W.; Xu, J.; Meng, F. Formation processes and source contributions of ground-level ozone in urban and suburban Beijing using the WRF-CMAQ modelling system. *J. Environ. Sci.* **2023**, *127*, 753–766. [CrossRef]
34. Georgiou, G.K.; Christoudias, T.; Proestos, Y.; Kushta, J.; Pikridas, M.; Sciare, J.; Savvides, C.; Lelieveld, J. Evaluation of WRF-Chem model (v3.9.1.1) real-time air quality forecasts over the Eastern Mediterranean. *Geosci. Model. Dev.* **2022**, *15*, 4129–4146. [CrossRef]
35. Chelhaoui, Y.; El Ass, K.; Lachatre, M.; Bouakline, O.; Khomsi, K.; Moussaoui, T.E.; Arrad, M.; Eddaif, A.; Albergel, A. A new optimized hybrid approach combining machine learning with WRF-CHIMERE model for PM10 concentration prediction. *Model. Earth Syst. Environ.* **2024**, *10*, 5687–5701. [CrossRef]
36. Mak, H. Improved Remote Sensing Algorithms and Data Assimilation Approaches in Solving Environmental Retrieval Problems. Ph.D. Thesis, The Hong Kong University of Science and Technology, Hong Kong, China, 2019. [CrossRef]
37. Krajčovičová, J.; Matejovičová, J.; Nemček, V. High-resolution residential emission model for use in the air quality modelling. *Meteorol. J.* **2020**, *23*, 1.
38. Geletič, J.; Benešová, N.; Belda, M.; Eben, K.; Huszar, P.; Jurus, P.; Krc, P.; Resler, J.; Vlček, O. FUME—A New Open Source Emission Processor for Air Quality Models. In Proceedings of the Air Quality 2018, Barcelona, Spain, 12–16 March 2018. [CrossRef]
39. Šedivá, T. Comparison of Emission Profiles in the CMAQ Model, Konferencia Mladých Odborníkov SHMU (Conference of Young Specialists of Slovak Hydrometeorological Institute) November 2021. Available online:: https://kmo.shmu.sk/media/files/archiv/2021/Meteorologia_klimatologia_a_kvalita_ovzdusia/Sediva_Tereza-Comparison_of_emission_profiles_in_the_CMAQ_model.pdf (accessed on 27 August 2024).
40. Kuenen, J.J.P.; Visschedijk, A.J.H.; Jozwicka, M.; Denier van der Gon, H.A.C. TNOMACC_II emission inventory; A multi-year (2003–2009) consistent high-resolution European emission inventory for air quality modelling. *Atmos. Chem. Phys.* **2014**, *14*, 10963–10976. [CrossRef]
41. Builtjes, P.J.H.; van Loon, M.; Schaap, M.; Teeuwise, S.; Visschedijk, A.J.H.; Bloos, J.P. *The Development of an Emission Data over Europe and Further Contributions of TNO-MEP*; Freie Universität Berlin, Institut für Meteorologie, Troposhärische Umweltforschung: Berlin, Germany, 2002.
42. Yarwood, G.; Jung, J.; Whitten, G.; Heo, G.; Mellberg, J.; Estes, M. Updates to the Carbon Bond Mechanism for Version 6 (CB6). In Proceedings of the 9th Annual CMAS Conference, Chapel Hill, NC, USA, 11–13 October 2010; pp. 1–4.
43. United States Environmental Protection Agency. Overview of AERO7 and AERO7i. CMAQ User's Guide v5.3. 2021. Available online: https://github.com/CMASCenter/EPA-CMAQ/blob/main/DOCS/Release_Notes/CMAQv5.3_aero7_overview.md (accessed on 24 September 2024).
44. Derková, M.; Neštiak, M.; Bellus, M.; Vivoda, J.; Španiel, O.; Dian, M.; Zehnal, R. Recent improvements in the ALADIN/SHMU operational system. *Meteorol. J.* **2017**, *20*, 45–52.
45. CAMS Global Atmospheric Composition Forecasts [Data]. Available online: https://ads.atmosphere.copernicus.eu/ (accessed on 27 August 2024).
46. CAMS European Air Quality Forecasts. Available online: https://ads.atmosphere.copernicus.eu/datasets (accessed on 27 August 2024).
47. Centrum Dopravního výZkumu, v. v. i. 2024. Available online: https://www.cdv.cz/en/ (accessed on 6 August 2024).
48. Geoportál. 2024. Available online: https://www.geoportal.sk/en/zbgis/zbgis/ (accessed on 7 August 2024).
49. Information System NEIS. Available online: https://www.air.sk/en/neis.php (accessed on 7 August 2024).
50. Copernicus Land Monitoring Service. CORINE Land Cover 2018 (Vector/Raster 100 m), Europe, 6-yearly. 2020. Available online: https://land.copernicus.eu/en/products/corine-land-cover/clc2018 (accessed on 7 August 2024).
51. Kuenen, J.; Dellaert, S.; Visschedijk, A.; Jalkanen, J.-P.; Super, I.; Denier van der Gon, H. CAMS-REG-v4: A state-of-the-art high-resolution European emission inventory for air quality modelling. *Earth Syst. Sci. Data* **2022**, *14*, 491–515. [CrossRef]
52. Guenther, A.B.; Jiang, X.; Heald, C.L.; Sakulyanontvittaya, T.; Duhl, T.; Emmons, L.K.; Wang, X. The Model of Emissions of Gases and Aerosols from Nature version 2.1 (MEGAN2.1): An extended and updated framework for modeling biogenic emissions. *Geosci. Model Dev.* **2012**, *5*, 1471–1492. [CrossRef]

53. Slovak Hydrometeorological Institute. Climatological Summary of January 2017 (Zhodnotenie Mesiaca Január 2017). Available online: https://www.shmu.sk/sk/?page=2049&id=805 (accessed on 30 August 2024).
54. Yang, Q.; Kim, J.; Cho, Y.; Lee, W.J.; Lee, D.W.; Yuan, Q.; Wang, F.; Zhou, C.; Zhang, X.; Xiao, X.; et al. A synchronized estimation of hourly surface concentrations of six criteria air pollutants with GEMS data. *NPJ Clim. Atmos Sci.* **2023**, *6*, 94. [CrossRef]
55. Lee, H.J.; Kim, N.R.; Shin, M.Y. Capabilities of satellite Geostationary Environment Monitoring Spectrometer (GEMS) NO_2 data for hourly ambient NO_2 exposure modeling. *Environ. Res.* **2024**, *261*, 119633. [CrossRef]
56. Mak, H.W.L.; Laughner, J.L.; Fung, J.C.H.; Zhu, Q.; Cohen, R.C. Improved Satellite Retrieval of Tropospheric NO_2 Column Density via Updating of Air Mass Factor (AMF): Case Study of Southern China. *Remote Sens.* **2018**, *10*, 1789. [CrossRef]
57. Handschuh J.; Erbertseder T.; Schaap M.; Baier F. Estimating PM2.5 surface concentrations from AOD: A combination of SLSTR and MODIS. *Remote Sens. Appl. Soc. Environ.* **2022**, *26*, 100716. [CrossRef]
58. Sentinel-5P. Available online: https://sentiwiki.copernicus.eu/web/s5p-mission (accessed on 27 August 2024).
59. World Health Organization. *WHO Global Air Quality Guidelines: Particulate Matter (PM2.5 and PM10), Ozone, Nitrogen Dioxide, Sulfur Dioxide and Carbon Monoxide*; World Health Organization: Geneva, Switzerland, 2021.

Disclaimer/Publisher's Note: The statements, opinions and data contained in all publications are solely those of the individual author(s) and contributor(s) and not of MDPI and/or the editor(s). MDPI and/or the editor(s) disclaim responsibility for any injury to people or property resulting from any ideas, methods, instructions or products referred to in the content.